Extrapolating fiber crossings from DTI data : can we gain the same information as HARDI?

EINDHOVEN UNIVERSITY OF TECHNOLOGY
Department of Mathematics and Computer Science

CASA-Report 10-20
March 2010

Extrapolating fiber crossings from DTI data. Can we gain the same information as HARDI?

by

V. Prčkovska, P.R. Rodrigues, R. Duits,
B.M. ter Haar Romeny, A. Vilanova

Centre for Analysis, Scientific computing and Applications
Department of Mathematics and Computer Science
Eindhoven University of Technology
P.O. Box 513
5600 MB Eindhoven, The Netherlands
ISSN: 0926-4507

Extrapolating fiber crossings from DTI data.
Can we gain the same information as HARDI?

V. Prčkovska[1], P.R. Rodrigues[1], R. Duits[1,2], B.M. ter Haar Romeny[1], and A. Vilanova[1]

[1] Department of Biomedical Engineering, [2] Department of Mathematics and Computer Science
Eindhoven University of Technology, WH 2.111, 5600 MB Eindhoven, The Netherlands
V.Prckovska@tue.nl

Abstract. High angular resolution diffusion imaging (HARDI) has proven to better characterize complex intra-voxel structures compared to its predecessor diffusion tensor imaging (DTI). However, the benefits from the modest acquisitions and significantly higher signal-to-noise ratios (SNRs) of DTI make it more attractive for use in clinical research. In this work we use contextual information derived from DTI data, to obtain similar crossing information as from HARDI data. We conduct synthetic phantom validation under different angles of crossing and different SNRs. We corroborate our findings from the phantom study to real human data. We show that with extrapolation of the contextual information the obtained crossings are the same as the ones from the HARDI data, and the robustness to noise is significantly better.

1 Introduction

The recent diffusion weighted magnetic resonance imaging (DW-MRI) technique, first introduced by Basser [1], diffusion tensor imaging (DTI), is subject of intense research mainly due to its feasibility in clinical practice (number of gradients (NG) around 20, b-value of 1000 s/mm^2 and total acquisition time of 3-5 minutes [2]). DTI constitutes a valuable tool to inspect fibrous structures in a non-invasive way. Despite the great potential for clinical applications, DTI has one obvious disadvantage due to the crude assumption for modeling the underlying diffusion process as Gaussian. In other words, in the areas of complex intra-voxel heterogeneity the DTI model fails to distinguish multiple fiber populations. This limits the accurate description of the diffusion process locally, and influences the accuracy of the fiber tracking algorithms, an important application of this model. To overcome the limitations of DTI, more complex acquisition schemes known as high angular resolution diffusion imaging (HARDI) were introduced [3]. These acquisitions come coupled with more sophisticated reconstruction techniques that tend to avoid any assumptions for the probability density function (PDF) that describes the underlying diffusion process. Thus, locally more accurate models for the diffusion process, that allow the detection of multiple fibrous structures, were introduced [4–9]. However, the increased accuracy in HARDI comes along with a few drawbacks, mainly in more

time consuming acquisitions (60 to few hundreds NG, higher b-values (> 2000 s/mm^2) and total acquisition times from 20 minutes to a few hours) [3,10]. This is one of the biggest impediments in applying HARDI in clinical setting. Another very important issue is the SNR in the images acquired by the typical DTI or HARDI acquisition protocols for clinical scanners. Despite the more accurate local modeling of the underlying diffusion process by the HARDI techniques, they require acquisitions at higher b-values and denser gradient sampling compared to DTI. Therefore, the acquired datasets have significantly lower SNRs than in DTI (especially in the diffusion weighted images which is sometimes a factor of 4 lower). The reconstructed diffusion profiles suffer from major noise pollution, that often produces false or displaced maxima of the reconstructed diffusion functions and might notably disturb the fiber tracking algorithms. Proper regularization techniques on the domain of these datasets are thus, important. However, there is an additional issue with the accuracy of the DW-MRI data. Since the noise is very prominent in the phase of an MRI signal, it is common to discard this information, thus considering only the amplitude. This results in anti-podally symmetric profiles as pointed by Liu et al. [11], that can only model single fiber or symmetric crossings of multiple fibers. However, this can not always be assumed to be the case in the white matter of the brain, especially in the structures as *optic chiasm*, *the hippocampus*, *the brain stem* and others. Since the data is ill defined, considering the contextual information (i.e., neighborhood) can be of outmost importance. There has been previous work on inter-voxel, contextual based filtering for estimating asymmetric diffusion functions [12] and cross-preserving smoothing of HARDI images [13], by modeling the stochastic processes of water molecules (i.e., diffusion) in oriented fibrous structures. However, these approaches increase the complexity of already complex and computationally heavy HARDI data. Rodrigues et al. [14], accelerated these complex convolutions enabling a fast framework for the noise removal, regularization and enhancement of HARDI datasets. Notwithstanding, contextual processing as described above has been applied only on HARDI models, due to the natural coupling of the space of positions and orientations that describe the diffusion process.

In this paper we address some of the above mentioned issues. We use data from typical clinically obtained DTI acquisitions to build spherical diffusion functions (SDF) that can be used for contextual processing of the data. The data initially comes with high SNR values making the local reconstruction of the SDFs reliable. The context information of well defined single direction fibers is extrapolated to areas where the fiber structure is considerably complex and therefore not defined in DTI. We analyze the difference of the contextually modified SDFs compared with the Qball reconstructions [15] from the same DW-MRI data.

2 Methods

In this section we present our method for creating extrapolated SDFs (E-SDFs) from diffusion tensors (DT) estimated from our DW-MRI data. We additionally give details on the contextual image processing and perform an evaluation.

2.1 Creating spherical diffusion functions from diffusion tensors

In DTI, the signal decay is assumed to be mono-exponential [16], and yields the equation:

$$S_g = S_0 \exp(-b\mathbf{g}^T\mathbf{D}\mathbf{g}) \tag{1}$$

where S_g is the signal in the presence of diffusion sensitizing gradient, and S_0 is the zero-weighted baseline signal, b-value is the parameter of the scanner closely related to the effective diffusion time, and the strength of the gradient field, $\mathbf{g}$ are the diffusion gradient vectors, and $\mathbf{D}$ is the 2^{nd} order symmetric, positive definite diffusion tensor (DT). Once the DT is calculated per voxel, the spherical diffusivity function (SDF) can be reconstructed, and sampled on the sphere

$$SDF(\mathbf{n}) = \mathbf{n}^T\mathbf{D}\mathbf{n} \tag{2}$$

where $\mathbf{n}$ is the direction vector defined by the tessellation. Figure 1 shows a typical linear DT and the correspondent diffusivity profile sampled on a sphere (in our case icosahedron of order 4, 642 points on a sphere). Note that this SDF, since it is derived from the DT, does not hold any crossing information and should not be confused with the apparent diffusion coefficient (ADC) whose crossing information does not necessarily coincide with the underlying fiber population as pointed by Özarslan et al. [7].

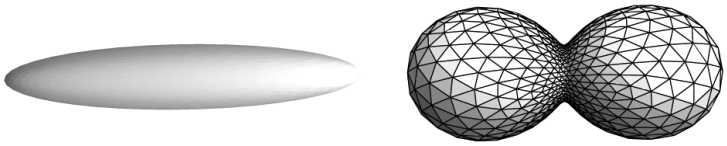

Fig. 1. A linear diffusion tensor (left) and the corresponding tessellated SDF (right).

Following Anonymous [14], from a tensor field, we create an SDF field, i.e., a HARDI-like dataset $\mathcal{U}$, a coupled space of positions and orientations:

$$\mathcal{U} : \mathbb{R}^3 \rtimes S^2 \to \mathbb{R}^+ : \mathcal{U}(\mathbf{y}, \mathbf{n}(\beta, \gamma)) \tag{3}$$

This means that on every position $\mathbf{y} \in \mathbb{R}^3$, the probability of finding a water particle in a certain direction $\mathbf{n}(\beta, \gamma)$ is given by a scalar. Here, β and γ are the spherical coordinates. To stress the coupling between orientation and positions we write $\mathbb{R}^3 \rtimes S^2$ rather than $\mathbb{R}^3 \times S^2$. Such an image $\mathcal{U}$ can now be enhanced. Throughout this article we consider DTI-data as the initial condition, which means that we set $\mathcal{U}(\mathbf{y}, \mathbf{n}) = \mathbf{n}^T\mathbf{D}(\mathbf{y})\mathbf{n}$.

2.2 Kernels for contextual enhancing of spherical diffusion functions

Duits [13,17] proposed a kernel implementation that solves the diffusion equation for HARDI images. The full derivation is beyond the scope of this manuscript. This kernel represents the Brownian motion kernel, on the coupled space $\mathbb{R}^3 \rtimes S^2$ of positions and orientations. Next, we present a close analytic approximation of the Green's function. This approximation is a product of two $2D$ kernels on the coupled space $p_{2D} : \mathbb{R}^2 \rtimes S^1 \rightarrow \mathbb{R}^+$ of 2D-positions and orientations:

$$\begin{aligned} &p_{3D}^{D_{33},D_{44},t}((x,y,z)^T, \mathbf{n}(\beta,\gamma)) \approx \\ &N(D_{33},D_{44},t) \cdot p_{2D}^{D_{33},D_{44},t}((z/2,x),\beta) \cdot p_{2D}^{D_{33},D_{44},t}((z/2,-y),\gamma) \ , \end{aligned} \tag{4}$$

where $\mathbf{y} = (x,y,z)^T$, and $N(D_{33},D_{44},t) \approx \frac{8}{\sqrt{2}}\sqrt{\pi}t\sqrt{tD_{33}}\sqrt{D_{33}D_{44}}$ takes care that the total integral over positions and orientations is 1. For details adhere to the work of Duits [13,17] and Rodrigues [14].

The diffusion parameters D_{33} and D_{44} and stopping time t allow the adaptation of the kernels to different purposes:

1. $t > 0$ determines the overall size of the kernel, i.e. how relevant is the neighborhood;
2. $D_{33} > 0$, the diffusion along the principal axis, determines how wide is the kernel;
3. $D_{44} > 0$ determines the angular diffusion, so the quotient D_{44}/D_{33}, models the bending of the fibers along which diffusion takes place.

We can now convolve this kernel with the SDF image $\mathcal{U}$, using the HARDI convolution [14], as expressed in equation 5. We chose the parameters for the kernel in order to give a high relevance to the diffusion along the principal axis $D_{33} = 0.6, D_{44} = 0.01$ and $t = 1.4$.

$$\Phi(\mathcal{U})[\mathbf{y},\mathbf{n}_k] = \sum_{\mathbf{y}' \in P} \sum_{\mathbf{n}' \in T} p_{\mathbf{y},\mathbf{n}_k}(\mathbf{y}',\mathbf{n}')\mathcal{U}(\mathbf{y}',\mathbf{n}') \ \Delta\mathbf{y}' \, \Delta\mathbf{n}' \tag{5}$$

where $p_{\mathbf{y},\mathbf{n}_k}$ is the kernel at position $\mathbf{y}$ and orientation $\mathbf{n}_k$, such that

$$p(R_{\mathbf{n}'}^T(\mathbf{y}-\mathbf{y}'), R_{\mathbf{n}'}^T\mathbf{n}_k) = p_{\mathbf{y},\mathbf{n}_k}(\mathbf{y}',\mathbf{n}') \tag{6}$$

and R is any rotation such that $R_{\mathbf{n}}\mathbf{e}_z = \mathbf{n}$. $\Delta\mathbf{y}'$ is the discrete volume measure and $\Delta\mathbf{n}'$ the discrete surface measure, which in case of (nearly) uniform sampling of the sphere, such as tessellations of icosahedrons, can reasonably be approximated by $\frac{4\pi}{|T|}$. P is the set of lattice positions neighboring to $\mathbf{y}$ and T is the set of tessellation vectors. The convolution with such a kernel will result on the extrapolation of crossing profiles where the neighborhood information so indicates, i.e., the E-SDFs.

In order to achieve the desired results, care should be taken on the sharpness of the input image $\mathcal{U}$. Before applying the convolution, the SDFs are min-max normalized and a power of 2 is employed to achieve a sharper version of the SDFs.

2.3 Data

Synthetic Data - To validate and analyse our methodology artificial datasets were generated. DT datasets were created where two fiber bundles forming 'tubes' with radii of 2 voxels intersect each other. Here, the tensors, with eigenvalues $\lambda = [17, 3, 3] \times 10^{-3} mm^2/s$ and oriented tangentially to the center line of the tube, are estimated using a mixed tensor model [5]. Gaussian noise with different SNRs, is added to the real and complex part of the signal reconstructed from equation 1. In order to evaluate the angular resolution we vary the angle between the two fiber tubes $\theta \in \{50°, 60°, 70°\}$, while keeping a constant $SNR = 20$. We made a choice for these angles, given that the accuracy of Qball to detect multiple fiber orientations, especially at low b-values, is around 60° [18]. In order to evaluate the robustness to noise, we fix the angle to θ=70°, and we vary the SNR $\{5, 10, 20\}$.

Real Human Data - Diffusion acquisitions were performed using a twice focused spin-echo echo-planar imaging sequence on a Siemens Allegra 3T scanner, with FOV 208 × 208 mm, isotropic voxels of 2mm. 10 horizontal slices were positioned through the body of the *corpus callosum* and *centrum semiovale*. Uniform gradient direction scheme with 49 directions was generated with the electrostatic repulsion algorithm [19] and the diffusion-weighted volumes were interleaved with b_0 volumes every 12^{th} scanned gradient direction. Dataset was acquired at b-values of 1000 s/mm^2.

3 Results

On figure 2 we present the results of the performance of the proposed E-SDFs compared to the Qballs [15] for different angles of crossings. We fix the SNR to 20, as in a typical DTI acquisition. We observe that for the angle of 50°, E-SDFs and the Qball fail to find multiple maxima in the crossing areas. For the angle of 60° the performance of E-SDFs (angular error of 55° with standard deviation of 12°) is as for Qball truncated at order of spherical harmonics $l = 6$ (angular error of 54° with standard deviation of 15°). At angle of 70°, the E-SDFs (angular error of 12° with standard deviation of 5°) outperform the best Qball scenario at order $l = 8$ (angular error of 24° with standard deviation of 8°).

Figure 3 demonstrates the robustness to noise of the E-SDFs, compared to Qballs of order $l = 6$. At higher order of truncation Qball performs much worse, giving many false positives in the linear areas where the SNR is low. We observe that regardless the SNR, the E-SDFs preserve the coherence of the linear and crossing regions, and preserve the angular error, to almost constant (see the plot on figure 3).

The *centrum semiovale* was used to illustrate the qualitative analysis of the classification results. It is an interesting region for analysis, since fibers of the *corpus callosum* (CC), *corticospinal tract* (CST), and *superior longitudinal fasciculus* (SLF) form different two-fiber and three-fiber crossing configurations in that area. The region-of-interest (ROI) was defined on a coronal slice (see figure 4 a). Even though the crossing information is missing in the original data, as

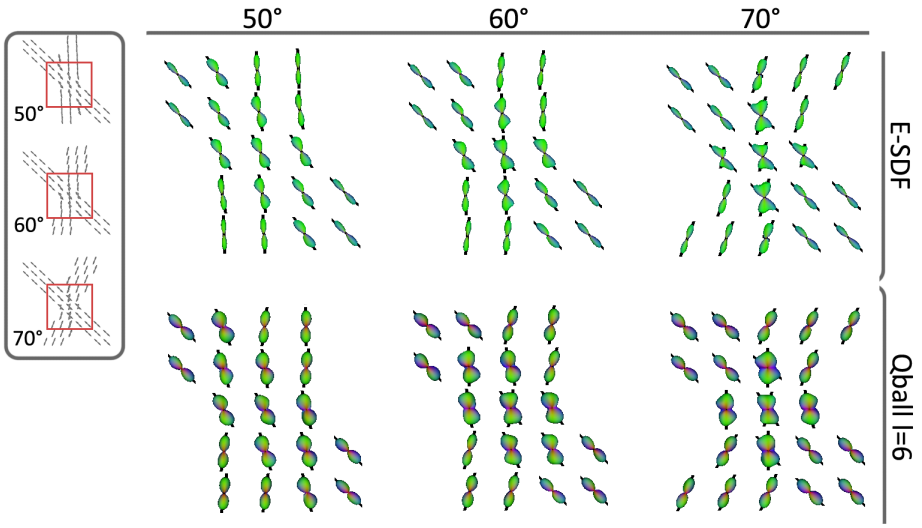

Fig. 2. E-SDFs and Qballs for different angles of crossing at fixed SNR=20.

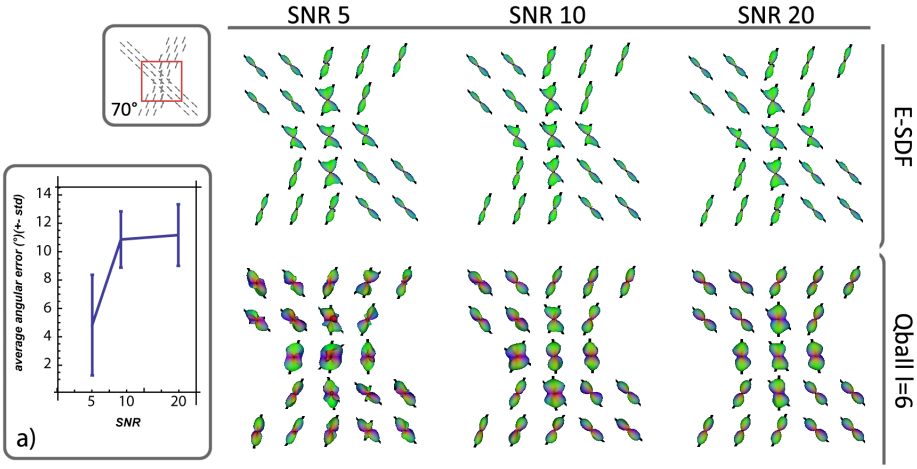

Fig. 3. E-SDFs and Qballs for different SNRs at fixed angle of 70°. a) plot of the angular error and standard deviation for the E-SDFs.

well as the created SDFs (figure 4 a and figure 4 b respectively), we observe that after the processing of the DTI data the crossing information is extrapolated (see figure 5 b) and very much comparable to the Qball reconstructions of order $l = 4$ from the same DW-MRI data. The benefits of the regularization feature of the contextual processing are also evident in figure 5 b, where clearly can be

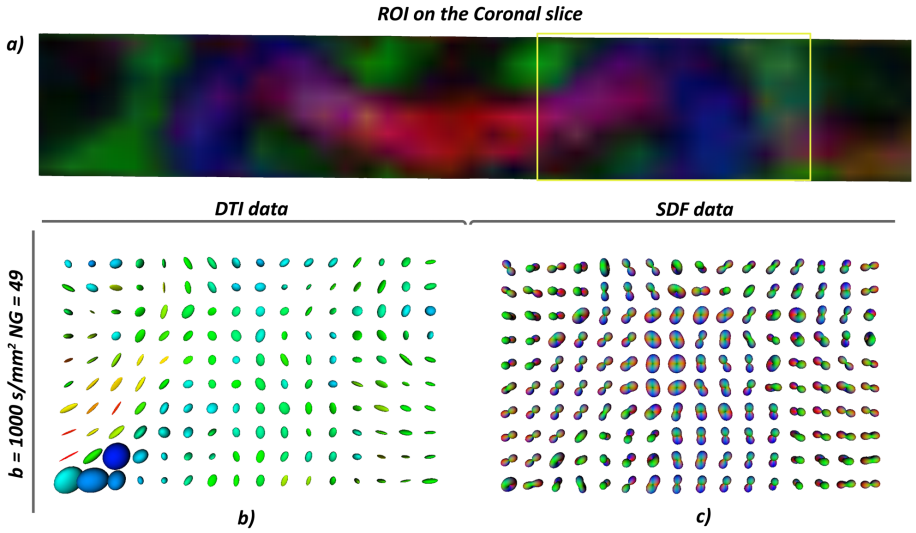

Fig. 4. The *centrum semiovale*. Left: the original DTI data, color coded by FA. Right: the SDFs from the DTI data, RGB color coded by orientation and min-max normalized.

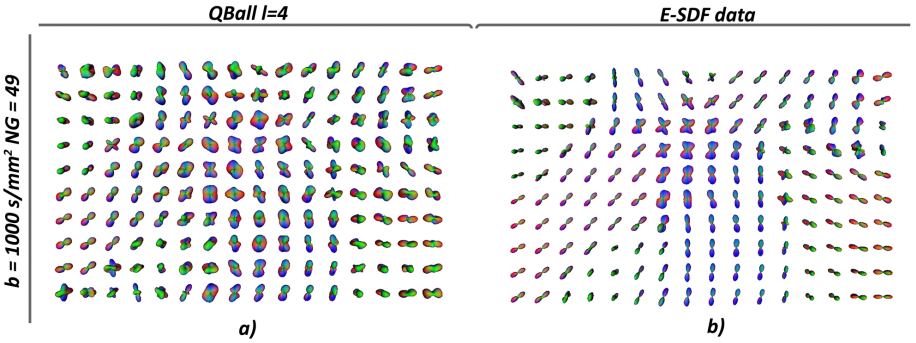

Fig. 5. Left: Qball of order 4. Right: E-SDFs of the same region.

observed the structure of CR intersecting the CC. This becomes more prominent compared to Qball truncated at higher l-order.

4 Conclusions and Future Work

In this work we presented a method for extrapolating crossing information using image processing of the coupled space of positions and orientations in DTI data. We show that with typical acquisition schemes for DTI, the local diffusion information gain can be similar as 6^{th} order Qball. The robustness to noise of the presented method is significantly better than from the Qballs reconstructed

from the same data. The main contribution from this work lies on demonstrating that modest acquisitions modeled by DTI, and using contextual information can result on the same information gain as in some of the popular HARDI reconstruction techniques that require more expensive acquisitions. The chosen kernel sets an overall reasonable probabilistic model that governs how the context of a fiber fragment is taken into account. Consequently, our framework lacks adaptivity. Future work addresses more adaptive fiber context models to the data, such that context is only included where it is required by the data. Future work should additionally bear more extensive validation to assess the exact differences between HARDI models and E-SDFs concerning acquisition parameters and anatomical areas of the brain.

References

1. Basser, P.J., Mattiello, J., Lebihan, D.: MR diffusion tensor spectroscopy and imaging. Biophys. J. **66**(1) (January 1994) 259–267
2. Jones, D.K.: The effect of gradient sampling schemes on measures derived from diffusion tensor mri: a monte carlo study. Magn Reson Med **51**(4) (2004) 807–15
3. Tuch, D.S.: Diffusion MRI of complex tissue structure. PhD thesis, Harvard (2002)
4. Frank, L.R.: Characterization of anisotropy in high angular resolution diffusion-weighted mri. Magn Reson Med **47**(6) (2002) 1083–99
5. Alexander, D.C., Barker, G.J., Arridge, S.R.: Detection and modeling of non-gaussian apparent diffusion coefficient profiles in human brain data. Magn Reson Med **48**(2) (2002) 331–40
6. Tuch, D.: Q-ball imaging. Magn. Reson. Med. **52** (2004) 1358–1372
7. Özarslan, E., Shepherd, T.M., Vemuri, B.C., Blackband, S.J., Mareci, T.H.: Resolution of complex tissue microarchitecture using the diffusion orientation transform (DOT). NeuroImage **36**(3) (July 2006) 1086–1103
8. Tournier, J.D., Calamante, F., Connelly, A.: Robust determination of the fibre orientation distribution in diffusion MRI: non-negativity constrained super-resolved spherical deconvolution. NeuroImage **35**(4) (2007) 1459–72
9. Jian, B., Vemuri, B.C.: A unified computational framework for deconvolution to reconstruct multiple fibers from Diffusion Weighted MRI. IEEE Transactions on Medical Imaging **26**(11) (2007) 1464–1471
10. M.Descoteaux: High Angular Resolution Diffusion MRI: From Local Estimation to Segmentation and Tractography. PhD thesis, Harvard (2008)
11. Liu, C., Bammer, R., Acar, B., Moseley, M.E.: Characterizing non-gaussian diffusion by using generalized diffusion tensors. Magn Reson Med **51**(5) (2004) 924–37
12. A. Barmpoutis, B. C. Vemuri, D.H., Forder, J.R.: Extracting tractosemas from a displacement probability field for tractography in dw-mri. In LNCS 5241, MICCAI (6-10 September 2008) 9–16
13. Duits, R., Franken, E.: Left-invariant diffusions on $\mathbb{R}^3 \rtimes S^2$ and their application to crossing-preserving smoothing on HARDI-images. CASA report, TU/e, nr.18 (2009) Available on the web *http://www.win.tue.nl/casa/research/casareports/2009.html*.
14. P. Rodrigues, R. Duits, B.t.H.R., Vilanova, A.: Accelerated diffusion operators for enhancing dw-mri. Research Report (2010) Available on the web `http://www.win.tue.nl/casa/research/casareports/2009.html`.

15. Descoteaux, M., Angelino, E., Fitzgibbons, S., Deriche, R.: Regularized, fast and robust analytical q-ball imaging. Magn. Reson. Med. **58** (2007) 497–510
16. Basser, P.J., Mattiello, J., Lebihan, D.: Estimation of the effective self-diffusion tensor from the nmr spin echo. Journal of Magnetic Resonance **Series B 103** (1994) 247–254
17. Duits, R., Franken, E.: Left-invariant diffusions on the space of positions and orientations and their application to crossing-preserving smoothing of HARDI images. Invited submission to International Journal of Computer Vision 2010 (2010) Available on the web `http://www.win.tue.nl/casa/research/casareports/2009.html`.
18. Prčkovska, V., Roebroeck, A.F., Pullens, W., Vilanova, A., ter Haar Romeny, B.M.: Optimal acquisition schemes in high angular resolution diffusion weighted imaging. In: MICCAI. Volume 5242 of LNCS., Springer (2008) 9–17
19. Jones, D., Horsfield, M., Simmons, A.: Optimal strategies for measuring diffusion in anisotropic systems by magnetic resonance imaging. Magn Reson Med **42** (1999) 515–525

PREVIOUS PUBLICATIONS IN THIS SERIES:

Number	Author(s)	Title	Month
10-16	R. Mirzavand A. Abdipour W.H.A. Schilders G. Moradi M. Movahhedi	LOD-FDTD method for physical simulation of semiconductor devices	March '10
10-17	I.M. Machyshyn P.H.M. Bovendeerd A.A.F. van de Ven P.M.J. Rongen F.N. van de Vosse	Stability against dynamic remodeling of an arterial tissue	March '10
10-18	I.M. Machyshyn P.H.M. Bovendeerd A.A.F. van de Ven P.M.J. Rongen F.N. van de Vosse	A model for arterial adaptation combining microstructural collagen remodeling and 3D tissue growth	March '10
10-19	T.L. van Noorden A. Muntean	Homogenization of a locally-periodic medium with areas of low and high diffusivity	March '10
10-20	V. Prčkovska P.R. Rodrigues R. Duits B.M. ter Haar Romeny A. Vilanova	Extrapolating fiber crossings from DTI data. Can we gain the same information as HARDI?	March '10

Ontwerp: de Tantes,
Tobias Baanders, CWI